J. Fluid Mech. (1970), *vol.* 42, *part* 2, *pp.* 309–320
Printed in Great Britain

On the transition to turbulent convection. Part 2. The transition to time-dependent flow

By RUBY KRISHNAMURTI
Geophysical Fluid Dynamics Institute, Florida State University

(Received 7 July 1969)

The Rayleigh number at which steady convective flow changes to time-dependent flow is determined experimentally for several fluids with Prandtl numbers from 1 to 10^4. The time dependence is of two forms: (i) a slow tilting of the cell boundary, with time scale of the vertical thermal diffusion time, (ii) an oscillation with a faster time scale determined by the orbit time of the fluid around the cell. The nature of this oscillation is one of hot (or cold) spots advected with the original cellular motion. At a fixed point in the fluid this produces a time periodic oscillation of the temperature. A discrete change of slope of the heat flux curve accompanies this transition. As the Rayleigh number is increased, transition to disorder is seen to result from an increase in the frequency and number of these oscillations.

Introduction

In a horizontal convecting layer of fluid, a number of discrete transitions occur before the flow becomes fully turbulent (Malkus 1954*a*). The first is the well-known transition at the critical Rayleigh number R_c from the conduction state to a state of steady two-dimensional convection. A small non-linear neighbourhood of R_c is reasonably well understood, but the Rayleigh number range between this and the turbulent state has received relatively little attention. Yet it is this intermediate range which would yield information on the mechanism of transition to turbulence. In part 1 (Krishnamurti 1970) it was found that the second transition, near $12R_c$, is one from steady two-dimensional to steady three-dimensional flow. This change in flow pattern is accompanied by a discrete change of slope of the heat flux curve.

The purpose of this paper is to report on experimental studies of convection beyond the second transition. We shall be concerned with the onset and nature of the time dependence of convective flows. Reports in the literature of the occurrence of time-dependent convection vary by three orders of magnitude in the Rayleigh number. This was in part due to a dependence upon Prandtl number Pr, which was pointed out by Rossby (1966) and explored by Willis & Deardorff (1967) for $0{\cdot}71 \leqslant Pr \leqslant 57$. However, even after accounting for the Prandtl number dependence, there is still considerable scatter and disagreement in the data. Externally steady, fixed heat flux experiments were conducted to observe plan form, transition to time dependence and nature of the time dependence, as well as the Rayleigh number R and heat flux H, for $10^3 < R < 10^6$, and for Prandtl numbers in the range 1 to 10^4.

Apparatus and procedure

The convection tank and the auxilliary apparatus for the control and measurement of temperatures was as described in part 1. The convecting fluid occupied a region 51 cm by 49 cm with a variable depth of 2–5 cm. This fluid layer was bounded above and below by highly conducting metal boundaries, so that all flow visualization was from the side. The plan form, heat flux, and Rayleigh number, were determined in the manner described in part 1.

For each steadily maintained external condition, the steadiness or non-steadiness of the resulting flow was to be determined. This was found to be too difficult by simply observing moving tracers through the fluid since there were gentle time dependencies with time scales of the order of several minutes to several hours. In order to have a record of the flow at an earlier time against which to compare the flow at a later time, the following photographic technique was devised. The apparatus used is shown schematically in figure 1. Two narrow

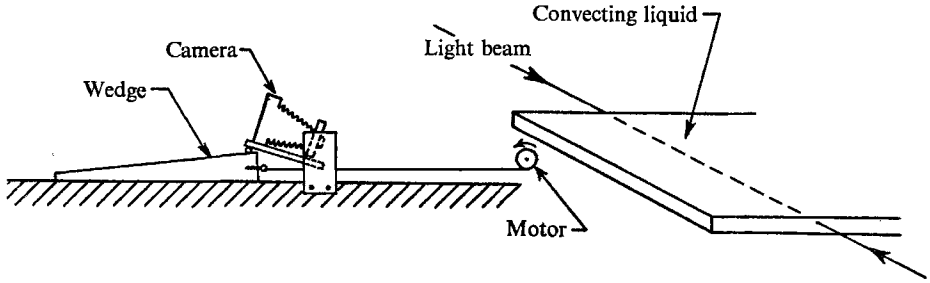

FIGURE 1. Apparatus for photographing the time evolution of flow.

overlapping beams of light from 2-watt sources illuminate aluminium flake tracers along a line in the x-direction, say, through the fluid. The beam was 2 to 3 mm in diameter (about one-tenth the depth of the fluid), and remained fixed in space throughout the observation time. The camera also remained at a fixed distance from the beam. However, the camera was free to rotate about an axis through its lens. With the camera aperture open, a synchronous motor drew a wedge under the back of the camera at a rate determined by the time scale of the time dependence of the flow. Thus, the photograph displays an (x, t) representation of the flow, where t is the time co-ordinate. At $t = 0$, the camera recorded alternating bright and dark regions, corresponding to the cellular structure, as a narrow strip of image across the film. When the flow was steady, the cell boundaries remained fixed in time, thus producing straight lines parallel to the t-axis on the photograph. With the beam near the top (or bottom) of the convecting layer, the tracer particles have an x-component of velocity which is given by the slope of the trajectories in the (x, t) representation. In order to study the nature of the time dependence, (x, t) photographs were obtained for the light beam at various horizontal positions, and at the following depths in the liquid: $z = 0$, $z = \pm 0{\cdot}25d$, $z = \pm 0{\cdot}4d$, where d is the layer depth, $z = 0$ is the mid-level.

To investigate further a time periodicity that was found in the (x, t) photographs, a sequence of time lapse photographs of a vertical slice through the

fluid layer were obtained. To study the thermal structure associated with this periodic flow, a quincunical array of thermocouples was introduced into the fluid in the following manner. A cylindrical plug of 1 in. diameter and 1 in. height was made of the same aluminium alloy as the boundary material. Five holes were drilled through the plug parallel to the cylinder generators in order to accommodate double-holed ceramic tubing. The holes of this tubing were just large enough to allow 30-gauge wires of copper and of constantan to be inserted. The holes as well as the thermocouple junctions were sealed by coating them with dissolved methyl methacrylate. The shortest distance between two thermocouple junctions was $\frac{5}{16}$ in. This plug with the thermocouples replaced another plug without thermocouples at the centre of the upper plate bounding the fluid layer. The plug was inserted to be flush with the upper plate and acted as part of the upper boundary. The five thermocouples, each 0·5 mm in diameter, extended 1·6 mm into the fluid. The plug was turned in such a way that three thermocouple junctions defined a line parallel to the x-direction (the direction of the light beam). Temperatures and temperature differences between points were measured as a function of the time and synchronized with the (x, t) photographs of the flow in the vicinity of the thermocouples. The most sensitive range of the amplifier was 0·3 μV full scale.

The procedure for obtaining the data was as described in part 1. Externally steady, fixed heat flux conditions were maintained, then temperature measurements and photographs were obtained. Next, the heat flux was increased by a few percent and the procedure was repeated. Hysteresis effects were also studied in the manner described in part 1.

Temperature differences across the fluid were kept as small as possible in an attempt to minimize non-Boussinesq effects. Temperature differences were at most several centigrade degrees. Also, all experiments were performed by heating and cooling symmetrically about room temperature.

A check was made in some cases to see if the aspect ratio affected the transition point to time dependence. The height to width ratio was varied from 0·02 to 0·04, both of which are very small values. Larger changes could not be made since this would require either such small temperature differences that measurement and control were made too difficult, or such large temperature differences that non-Boussinesq effects would become significant.

The entire procedure was repeated for seven fluids having Prandtl numbers 0·71, 6·7, 57, $1{\cdot}0 \times 10^2$, $0{\cdot}86 \times 10^3$, $0{\cdot}85 \times 10^4$. The properties of these fluids are described in table 1 of part 1.

Experimental results

A typical plot of heat flux *versus* Rayleigh number is shown in figure 2. The heat flux has been scaled so that it is the product of Nusselt and Rayleigh numbers. The data is very well represented by straight line segments of different slopes. In order of increasing R, the first transition occurs at the critical Rayleigh number R_c, the second occurs around $12R_c$. The third and fourth changes of slope, seen in figure 2, occur at Rayleigh numbers designated R_{III} and R_{IV}.

The value of R_{III} was found to be dependent upon Prandtl number. They are listed in table 1 for the cases in which R_{III} was approached from below. For the fluid of Prandtl number 2×10^2 only the change of flow was recorded. Columns 3 4, and 5 of table 1 summarize the heat flux data. As in part 1 the difference in magnitude of change of slope is not explained. It can only be suggested that the

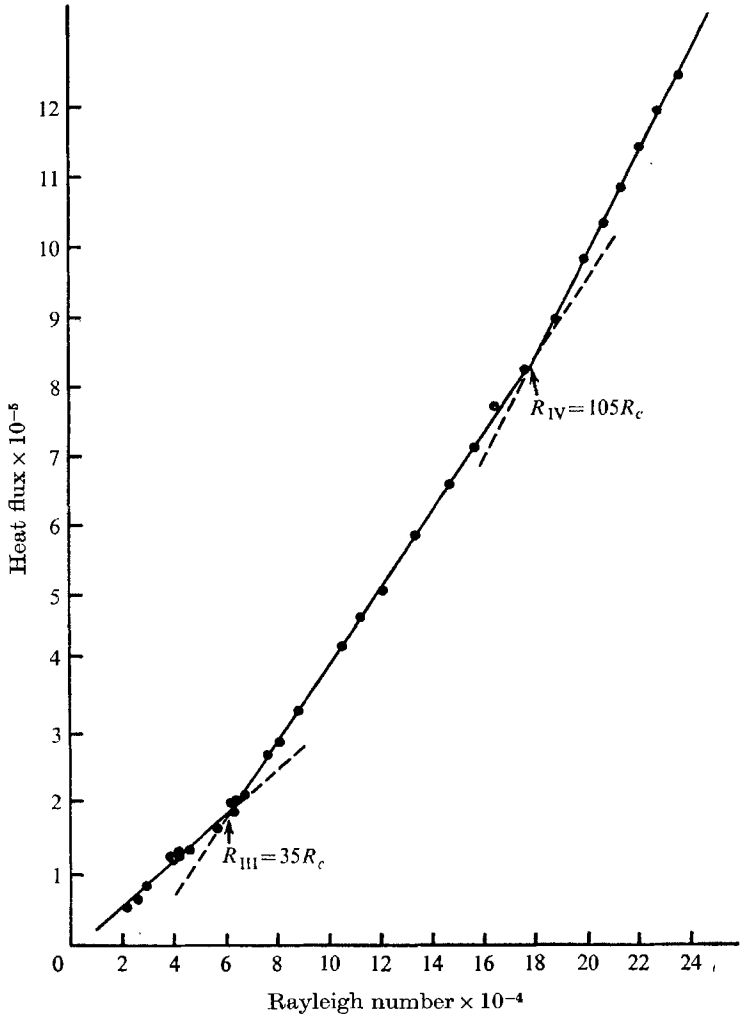

FIGURE 2. Heat flux *vs.* Rayleigh number, showing the third and fourth transitions. Heat flux curve, $Pr = 1{\cdot}0 \times 10^2$. The heat flux has been non-dimensionalized so that it is the product of Nusselt and Rayleigh numbers.

difference may depend upon past history since metastable states appear to be involved. Figure 3 shows the hysteresis in heat flux when R is increased, then decreased, through a sequence of externally steady states. The fourth change of slope was determined only for Prandtl number $1{\cdot}0 \times 10^2$, 0·71 and 6·7.

We next describe the results of the photographic studies of the flow. Although the plan form photographs are not synoptic pictures of the flow (since the time

required to produce such a photograph is comparable to the scale of the time dependence), they show that the flow is completely three-dimensional, much like figure 7 of part 1.

In searching for the Rayleigh number R_t at which the flow becomes time dependent, the following was noted. Of course externally steady conditions were attained before the steadiness of the flow was tested. This, in itself, required

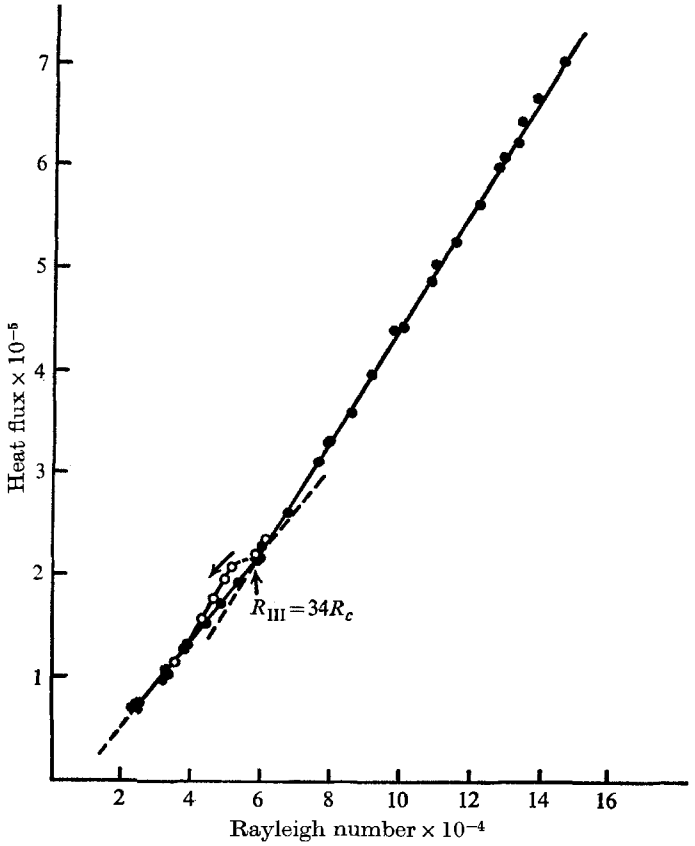

FIGURE 3. Heat flux *vs.* Rayleigh number, showing the third transition. Heat flux curve, showing hysteresis, $Pr = 0{\cdot}86 \times 10^3$. —●—●—●—, R increased; –O–O–, R decreased.

several vertical thermal diffusion times (d^2/κ). It was found that if the (x,t) photographs showed steady flows for at least one diffusion time, which was one hour in a particular case, then the flow was steady 10 or 20 h later also. Thus, in general, photographs were obtained for a duration of one diffusion time (one to seven hours in these experiments) to determine steadiness or non-steadiness of the flow.

A typical (x,t) photograph of steady flow is shown in figure 4(*b*) (plate 2). The lowest value of Rayleigh number, approached from below, for which the photographs show a time dependence was labelled R_t, and is shown in table 1 for comparison with R_{III}. In the case of air, Prandtl number 0·71, the labelling and association of the transitions become uncertain since the flow was not visualized.

Internal thermocouple traces show the flow to become time dependent around $2{\cdot}8R_c$. The heat flux transition closest to this value is the second at $2{\cdot}3R_c$.

The (x,t) photographs show the nature of the time dependence to be bimodal. One mode is a slow tilt of the cell boundary with a time scale d^2/κ for the layer. The result of this tilting is seen in figure 4 (*a*) (plate 1), for example. The other is an oscillatory mode seen, for example, in figure 4 (*f*) (plate 3). Of the several

Pr	R_{III}	Slope dH/dR $R < R_{III}$	Slope dH/dR $R > R_{III}$	Change of slope at R_{III}	R_t
0·71	—	—	—	—	$2{\cdot}8R_c$
6·7	$21R_c \pm 15\,\%$	4·4	4·8	0·4	$18R_c$
57	$30R_c \pm 25\,\%$	—	—	—	$28R_c$
$1{\cdot}0 \times 10^2$	$35R_c \pm 17\,\%$	3·4	5·6	2·2	$33R_c$
$2{\cdot}0 \times 10^2$	—	—	—	—	$33R_c$
$0{\cdot}86 \times 10^3$	$34R_c \pm 10\,\%$	4·0	5·6	1·6	$34R_c$
$0{\cdot}85 \times 10^4$	$31R_c \pm 10\,\%$	4·5	5·6	1·1	$33R_c$

TABLE 1

hundred points on the (R, Pr) plane that were studied, both modes were always present above R_{III}, never present below. The oscillatory mode has the following characteristics:

(i) With the light beam near the top or bottom boundary a bright region of strong shear (or 'knot') can be identified which moves laterally from one cell boundary to the other, and this phenomenon is repeated periodically with time. An example is seen in figure 4 (*f*) (plate 3). The knot is described as being advected with the flow, having approximately the same trajectory as the flow in cells without knots. There are, however, changes in curvature along its trajectory representing accelerations or decelerations. This is seen in figure 4 (*h*) (plate 4) in an expanded view of a few cells. Similar photographs are obtained near either the top or bottom boundary; at mid-level the knot is detectable but there is no cross-cell motion. This is seen in figures 4 (*c*) and (*d*) (plate 2), where in 4 (*d*) the beam was at mid-level, $z = 0$, while in 4 (*c*) the beam was at $z = 0{\cdot}4d$. All other parameters are equal. In view of the three-dimensional nature of the plan form it is clear that the light beam at $z = \pm 0{\cdot}4d$ will intersect regions in which the flow has no x-component but is entirely along the line of sight. Knots on such a flow appear periodically as a bright spot but do not display lateral motions.

Close-up photographs of a vertical slice through a few cells are arranged in a time-lapse sequence in figure 5 (plate 4). Each of the pictures is a 5 sec exposure taken at 15 sec intervals. The arrows indicate the progress of a bright region around a cell. It is an oscillation in the sense that an observer at a fixed point in the fluid will detect a time period behaviour of the flow. The period is related to the flow rate which increases with Rayleigh number. At these Rayleigh numbers the period is much shorter than d^2/κ for the layer. The observed period is plotted against R in figure 8.

The bright regions in the (x,t) photographs are interpreted as regions of strong shear rather than concentration of tracer. They could be seen as soon as

the flow was established after thorough stirring as well as after long periods of convection.

(ii) We now describe the statistical behaviour of knots in a collection of cells. Just above R_{III} perhaps only one cell of all the cells in the line across the tank displays oscillation during one thermal diffusion time. As R is increased, more and more cells display this oscillation at any instant. This is seen in the sequence

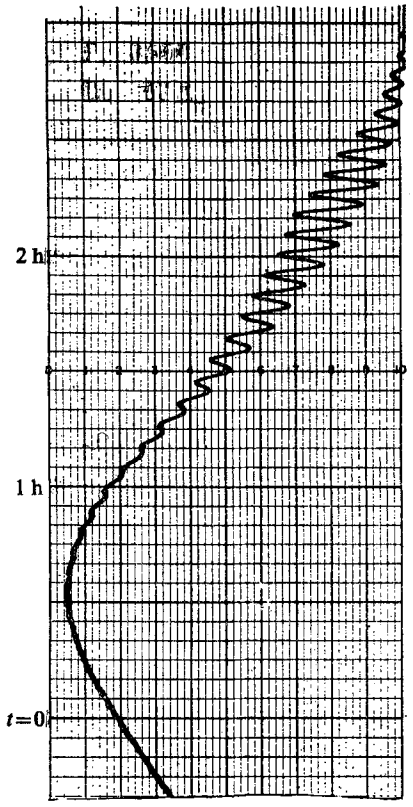

FIGURE 6. The temperature difference between two thermocouple junctions within the convecting fluid as it varies with time. The thermocouples are 0·79 cm apart and extend 1·6 mm into the fluid from the top boundary $R = 47R_c$, $Pr = 0{\cdot}85 \times 10^4$.

of figures 4(*c*) (plate 2), (*e*), (*f*), and (*g*) (plate 3) for Prandtl number 57. The oscillation in any particular cell disappears after approximately one thermal diffusion time, and appears in another cell, so that on the average the same number of cells display oscillation at a given R, Pr. At sufficiently high R, depending upon Prandtl number, almost all cells display oscillations at any instant. However, the phase becomes undistinguishable after a few oscillations. Transition to disorder appears to result from an increase in the number and frequency of these oscillations. The behaviour at other horizontal positions was statistically similar. For all the liquids studied with $6{\cdot}7 \leqslant Pr \leqslant 8500$, (x, t) photographs were obtained which displayed both the slow tilting and the faster oscillation.

(iii) We next describe some of the thermal properties of the time-dependent

flows. A typical trace of the temperature difference between two thermocouples in the fluid is shown in figure 6. Figure 7 (plate 5) shows a synchronized (x, t) photograph and the corresponding trace of the temperature difference between the middle and right-hand thermocouple. (Three of the five thermocouples are visible as three straight lines in the photographs.) An oscillation in the temperature difference occurs as the knots pass by the thermocouples. Similar photographs synchronized with the temperature traces show that a slow tilt of the

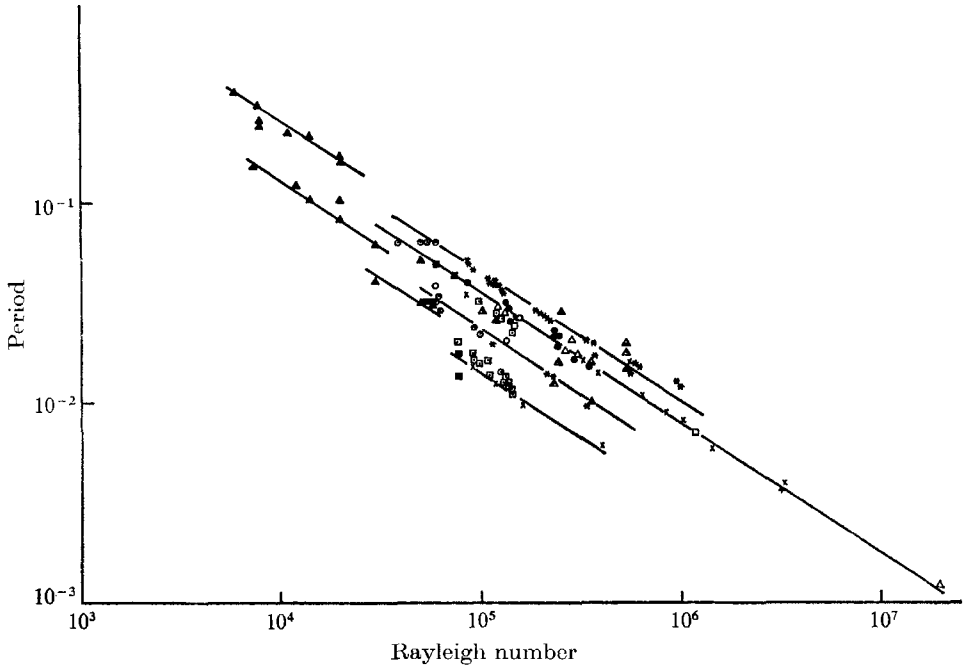

FIGURE 8. The period of oscillation plotted against Rayleigh number. The period has been non-dimensionalized by use of the thermal diffusion time d^2/κ.

	Rossby	Krishnamurti		Rossby	Krishnamurti
Pr = 0·71	—	▲	Pr = 194	×	⊠
= 6·7	○	⊙	= 400	+	—
= 39	●	—	= 860	□	⊡
= 57	—	*	= 8500	—	■
= 102	△	△			

cell wall is accompanied by a correspondingly slow change in temperature. The internal temperature traces showed oscillations with or without tracers in the fluid.

(iv) At some Rayleigh number greater than about R_{IV}, the doubled frequency of oscillations begins to appear. This is particularly noticeable in figure 4(*e*) (plate 3), where both 8 and 16 or 17 oscillations are observable in two different cells on the same photograph. The extension of the above arguments would be that twice as many knots are now advected with the flow. Traces of temperature at one point in the fluid, relative to a steady bath temperature also begin to

display this double frequency above R_{IV}. This phenomenon was observed by Rossby (1966) as well as by Willis & Deardorff (1967), and is seen in a plot of period *vs.* Rayleigh number in figure 8. Although this requires further exploration, it appears that the occurrence of the double frequency is associated with the heat flux transition at R_{IV}.

Variation of the aspect ratio from 0·02 to 0·04 produced no change in the transition point R_{III}. However, both these values are small; the layer is shallow in both cases.

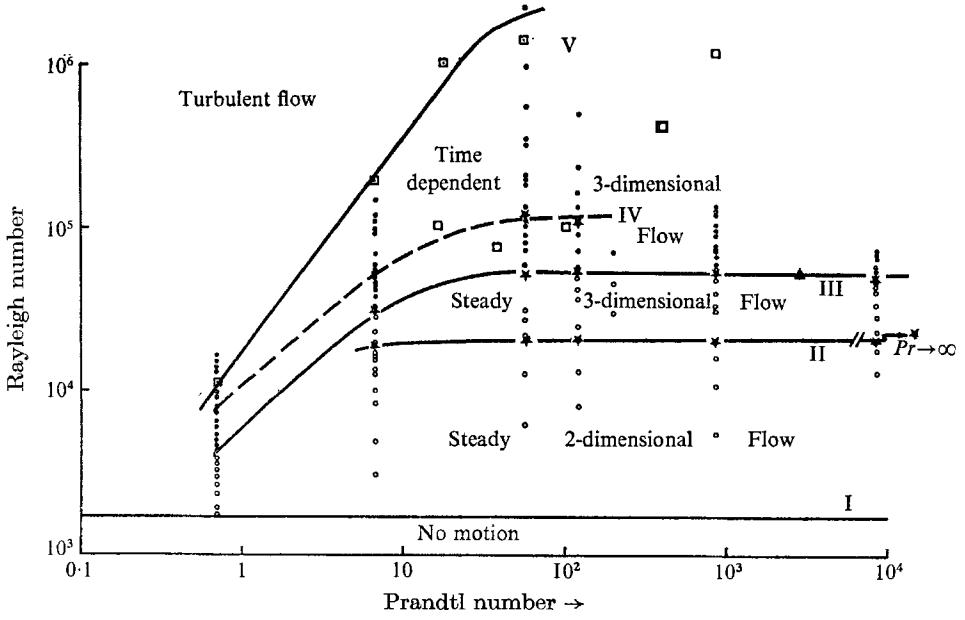

FIGURE 9. The régime diagram. The circles represent steady flows, the circular dots represent time-dependent flows. The stars represent transition points. The open squares are Rossby's observations of time-dependent flow, the squares with a dot in the centre are Willis & Deardorff's observations for turbulent flow. The triangle is Silveston's point of transition to time-dependent flow (see text).

The various régimes of flow observed are summarized in figure 9. The transition points, marked by stars, are for Rayleigh number increased from below. The complete diagram for R decreased from above has not been obtained, but some of these transitions can be seen in the heat flux curves. The details of the observations in each régime are as follows:

(i) The line labelled I marks the linearly predicted critical Rayleigh number R_c which is independent of Prandtl number. In the symmetric problem the flow above R_c is predicted and observed to be two-dimensional. There is a discrete change of slope of the heat flux curve associated with this transition.

(ii) The curve labelled II marks the transition from steady two-dimensional to steady three-dimensional flow. This transition was described in part 1, and is accompanied by a discrete change of slope also.

(iii) Curve III is defined by the Rayleigh number R_{III} at which a third change of slope occurs and above which the flow is time dependent. R_{III} depends upon

Prandtl number for $Pr \leqslant 50$, then approaches a constant value of $R_{\mathrm{III}} = 55{,}000$. Steady flows are indicated by circles, time-dependent flows by circular dots. This is in agreement with Silveston's (1958) observation for $Pr = 3 \times 10^3$, shown by a triangle in figure 9, for which he described the flow as 'constantly shifting'. This is also in agreement with Malkus's (1954*b*) observation for acetone, although he quotes two values with some spread. It is, however, not in agreement with Rossby's data (1966), shown by open squares in figure 9, although these latter may be interpreted as points at which the flow appeared turbulent. However, Rossby's data so interpreted would then be in disagreement with Willis & Deardorff's curve (shown by open squares with a dot and defining curve V) for occurrence of turbulent flows. Curve III is somewhat lower than Willis & Deardorff's (1967) corresponding curve for Prandtl numbers 0·71 to 57. This is understandable from two considerations. With only one temperature probe to determine time dependence, one may have to wait many diffusion times before an oscillation occurred at the probe. However, in their experiments the Rayleigh number changed considerably in one diffusion time. Also, in view of this external unsteadiness, they discarded the slower time dependence with the thermal diffusion time scale.

(iv) The curve labelled IV has been studied less extensively. The change of slope at R_{IV} has been observed for the fluids with Prandtl numbers 0·71, 6·7, and $1{\cdot}0 \times 10^2$. For Prandtl number 57 only the occurrence of the double frequency was noted.

Discussion of the observations

Much of this study has been to identify the various régimes of convective flow. Although all aspects of the time dependence have not been discussed, the study of the oscillatory behaviour may be summarized as follows. Regions of strong shear or 'knots' have been identified. The (x, t) photographs show that these knots are very nearly advected with the cellular convective flow. The internal temperature measurements synchronized with the (x, t) photographs show that the knots correspond to temperature anomalies. These knots persist for a time of the order of the vertical thermal diffusion time. The description of the time-dependent flow as hot or cold spots advected around the cell by the mean flow fits very well with Welander's model (Keller 1966; Welander 1967) of oscillatory convection. With a model of convection in a tubular loop they describe the conditions under which a relaxation oscillation can occur. The model consists of a tube of fluid closed into a loop in a vertical plane. The heat flux through the walls of the tube is specified as follows. Heat is supplied at a point along the bottom of the loop, and removed at a point along the top of the loop. The magnitude of the heat transferred depends upon the flow rate. No heat is allowed to flow across the walls on the vertical branches of the tube. Welander's parameter ϵ is equivalent to a Prandtl number, and his flow rate $\bar{q}$ would be a function of Rayleigh and Prandtl numbers. A steady flow of fluid around the loop is of course a possible solution. Welander shows that this flow is unstable in a certain range of parameters to an oscillatory disturbance. The physical mechanism is

understood as follows. A hot spot is imagined to form as a perturbation near the heat source. If the Prandtl number is sufficiently large (thermal diffusivity κ is small), and the Rayleigh number sufficiently large (so that the orbit time of a particle around the cell is small) then such a hot spot may be carried around the cell before losing its identity. Welander shows that because the hot spot has extra buoyancy, it creates, for a certain range of parameters, a maximum flow rate while passing the upper part of the loop and a minimum flow rate while passing the lower part of the loop. Thus, the heat sink becomes less efficient, the heat source becomes more efficient than in the case of flow without the hot spot. The initial hot spot receives a boost each time it passes the heat source, and is thus maintained. Similarly, a cold spot receives a boost each time it passes by the heat sink. At a fixed point within the fluid then, the temperature will oscillate regularly with time with a frequency given by the orbit time or twice the orbit time depending upon the number of temperature anomalies. Welander shows that below a critical Prandtl number this oscillatory instability cannot occur, and that for large Prandtl number varies as $\bar{q} \sim (Pr)^{\frac{1}{2}}$.

At very much smaller Prandtl numbers, turbulence arises presumably through shear instabilities. At very large Prandtl numbers there is the mechanism described by Howard (1966) of thermal instability of the boundary layer. This is apparently not the mechanism occurring in experiments with $1 \leqslant Pr \leqslant 10$ since, for these fluids, $3R_c \leqslant R_{\mathrm{III}} \leqslant 20R_c$. Even if the two thermal boundary layers, each of thickness δ, occupied one half the layer so that $\delta = \frac{1}{4}d$, the critical Rayleigh number for the boundary layer becomes 64 times that for the overall layer, which is difficult to reconcile with an instability at $3R_c$. Howard's theory is intended for higher Rayleigh and Prandtl numbers. However, even within the range of the experiments described in this paper, the mechanism of Howard's theory may complement that of Welander's theory.

It is not immediately obvious that the hot and cold spots on Welander's model will increase the heat flux. It may be stated, however, that an increased heat flux is observed to coincide with the appearance of these anomalies.

Welander's model may be extended to allow many hot and cold spots circulating around the cell provided the orbit time is sufficiently small (Rayleigh number sufficiently large) that each is rejuvenated before they diffuse into one another. An instantaneous picture of the temperature field would then be one with higher modes in the vertical (Malkus 1954*a*). However, it appears to be coincidental that for water and acetone the higher transitions correspond to instability points of higher vertical modes on the conduction profile since the observed transitions are in fact Prandtl number dependent.

Summary

Series of externally steady, fixed heat flux experiments were performed to measure Rayleigh number, heat flux and changes in flow for

$$0{\cdot}71 \leqslant Pr \leqslant 0{\cdot}85 \times 10^4 \quad \text{and} \quad 10^3 < Ra < 10^6.$$

The régime diagram summarizing these experiments is shown in figure 9. Each of the curves I, II, III and IV marks a transition with a change of slope in the

heat flux curve. Above curve III, the flow is time dependent with a slow tilting of the cell boundary and a faster oscillation which has the nature of hot or cold spots advected with the mean flow. Transition to disorder is seen to result from an increased number and frequency of such oscillations.

The paper is also part of Geophysical Fluid Dynamics Institute, Florida State University, Contribution 25. This research was supported at UCLA under Grant GP-2414 of the National Science Foundation, at Stanford University under a grant from the Office of Saline Water, and at the Florida State University under Office of Naval Research Contract N 00014-68-A-0159, where the largest part of the work was done. I am grateful to Professor W. V. R. Malkus, to Professor Andreas Acrivos, and to Professor Richard L. Pfeffer for this support.

REFERENCES

HOWARD, L. N. 1966 *Proceedings of the Eleventh International Congress on Applied Mechanics*, 1109–1115. Berlin: Springer.

KELLER, J. B. 1966 *J. Fluid Mech.* **26**, 599–606.

KRISHNAMURTI, R. 1970 *J. Fluid Mech.* **42**, 295.

MALKUS, W. V. R. 1954*a* *Proc. Roy. Soc.* A **225**, 185–195.

MALKUS, W. V. R. 1954*b* *Proc. Roy Soc.* A **225**, 196–212.

ROSSBY, H. T. 1966 Dissertation, M.I.T.

SILVESTON, P. L. 1958 *Forch. Ing. Wes.* **24**, 29–32, 59–69.

WELANDER, P. 1967 *J. Fluid Mech.* **29**, 17–30.

WILLIS, G. E. & DEARDORFF, J. W. 1967 *Phys. Fluids*, **10**, 931–937.

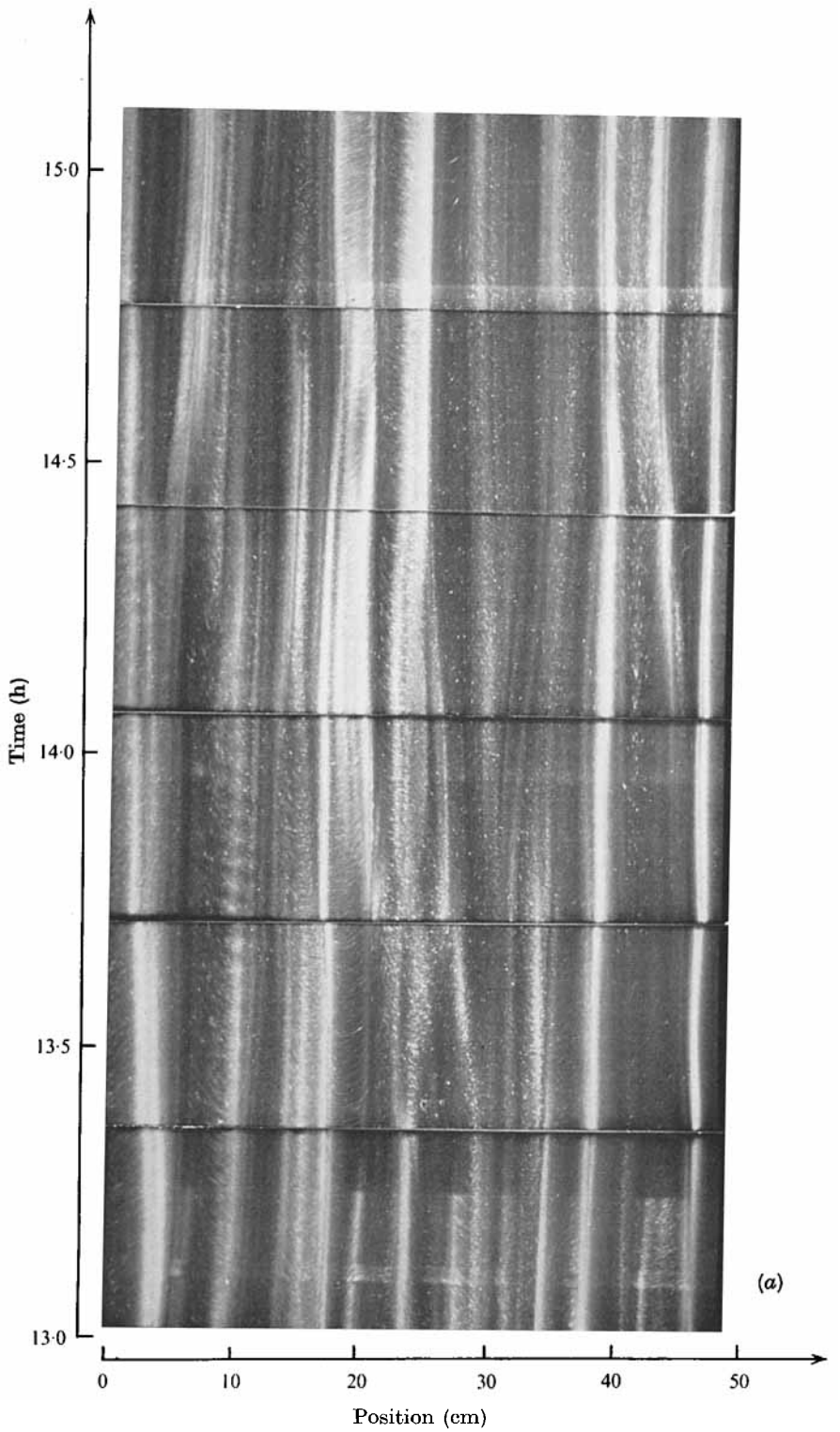

FIGURE 4. (x, t) photographs of convective flow. The position x through the tank is along the abscissa; the total width of the photograph represents 48 cm through the fluid. The time t is along the ordinate. (*a*) $R = 45R_c$, $Pr = 1{\cdot}0 \times 10^2$, $Z = 0{\cdot}4d$. The total time is 2·2 h.

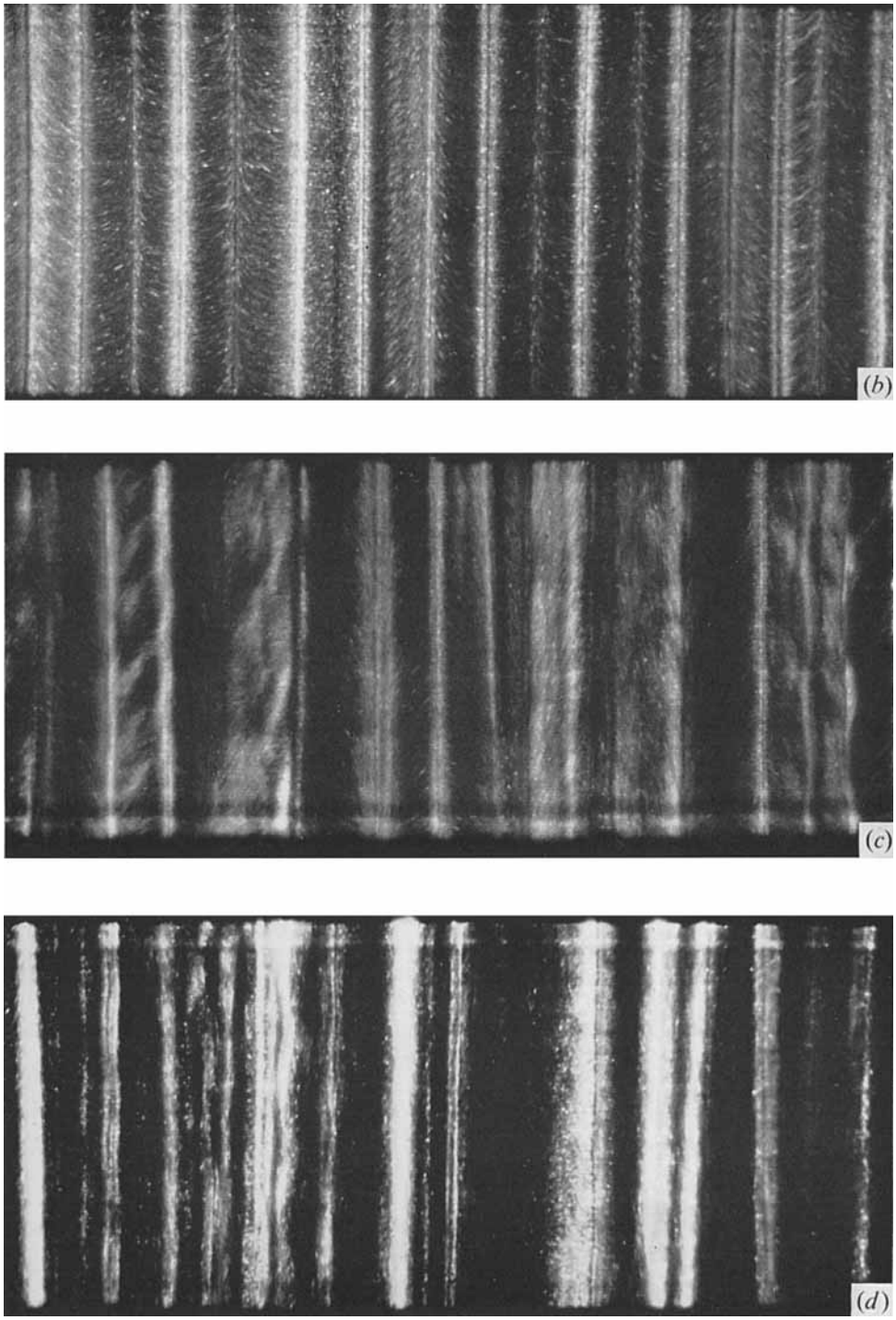

FIGURE 4 (*b*, *c*, *d*). (*b*) $R = 28R_c$, $Pr = 57$, $Z = 0{\cdot}4d$. The total time is 17 min. (*c*) $R = 123R_c$, $Pr = 57$, $Z = 0{\cdot}4d$. The total time is 6·4 min. (*d*) $R = 123R_c$, $Pr = 57$, $Z = 0$. The total time is 6·4 min.

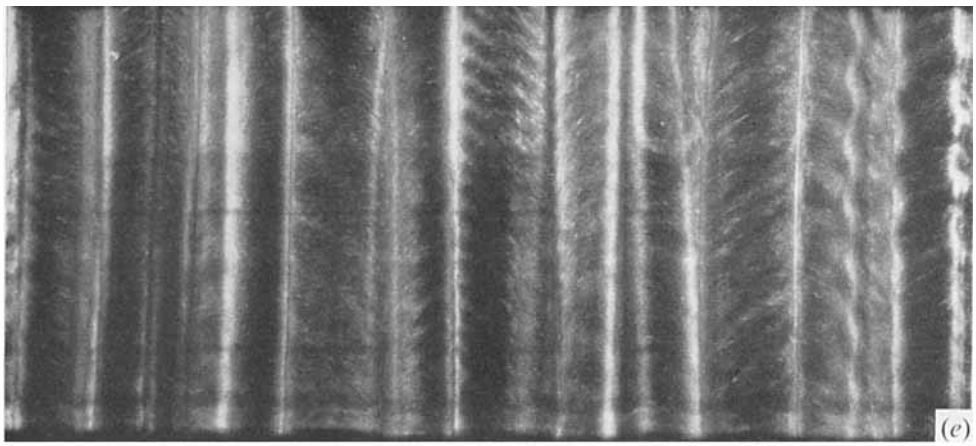

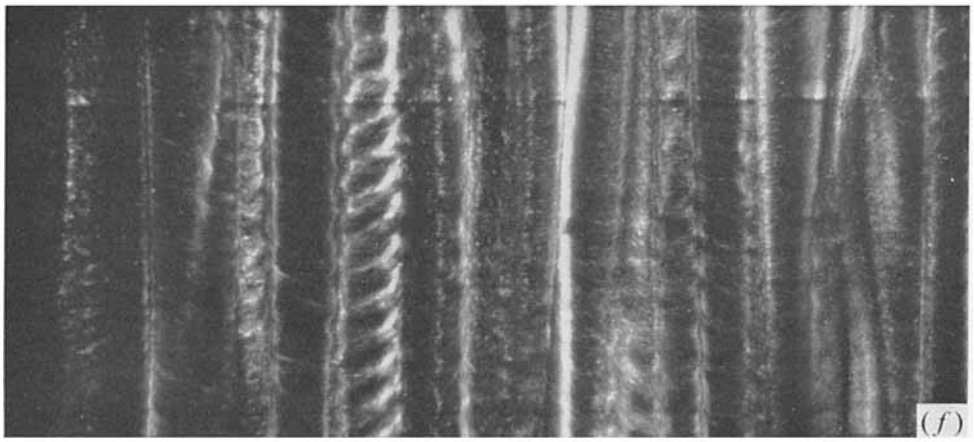

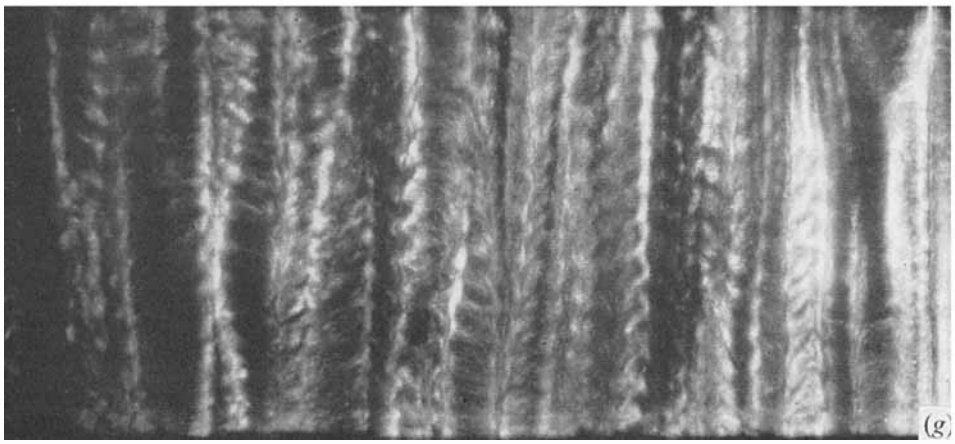

FIGURE 4 (*e*, *f*, *g*). (*e*) $R = 135R_c$, $Pr = 57$, $Z = -0{\cdot}4d$. The total time is 15 min. (*f*) $R = 200R_c$, $Pr = 57$, $Z = -0{\cdot}4d$. The total time is 17 min. (*g*) $R = 335R_c$, $Pr = 57$, $Z = -0{\cdot}4d$. The total time is 15 min.

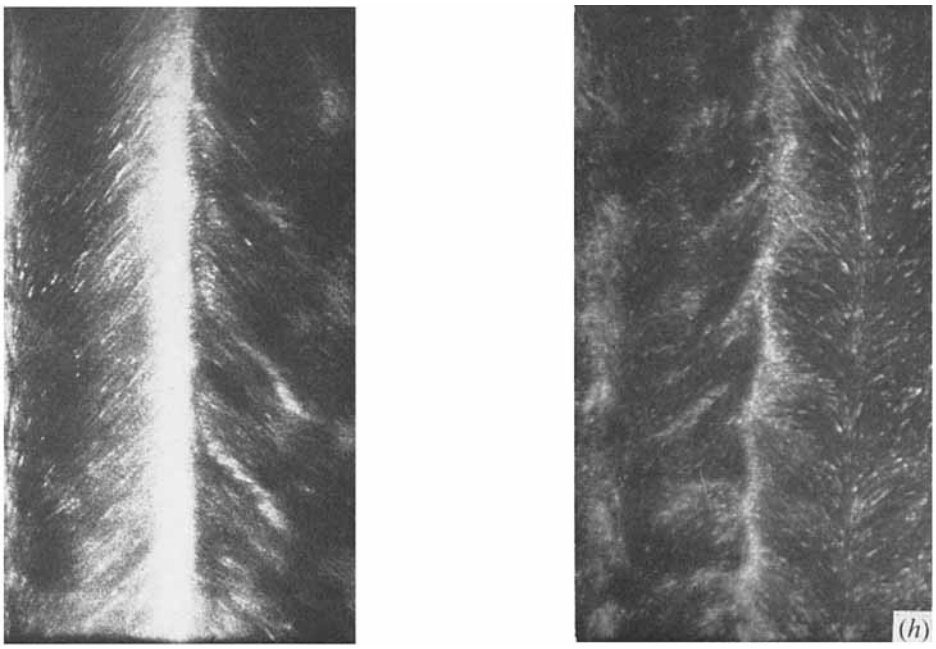

FIGURE 4 (*h*). Portions of (x, t) photographs showing the periodic nature of the flow in one cell. $R = 33R_c$ in the picture on the left, $R = 48R_c$ on the right; $Pr = 6{\cdot}7$. The total time is 7 min.

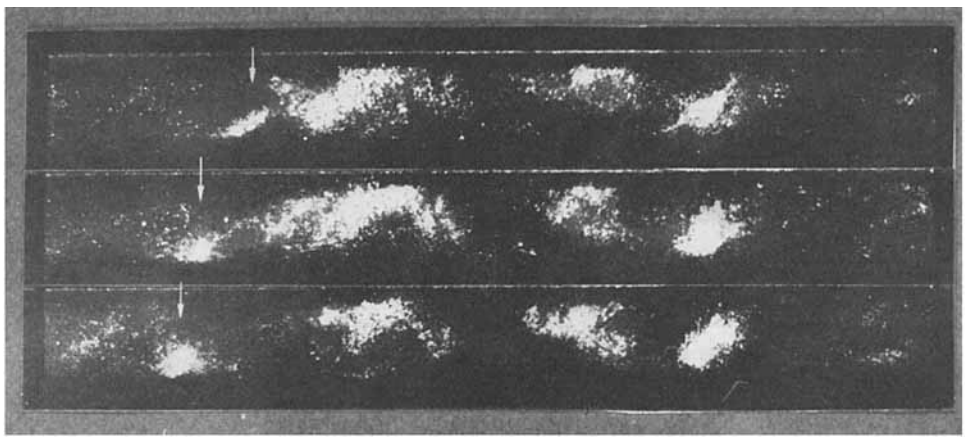

FIGURE 5. Time lapse photographs of a vertical section through several cells. $R = 67R_c$, $Pr = 6{\cdot}7$.

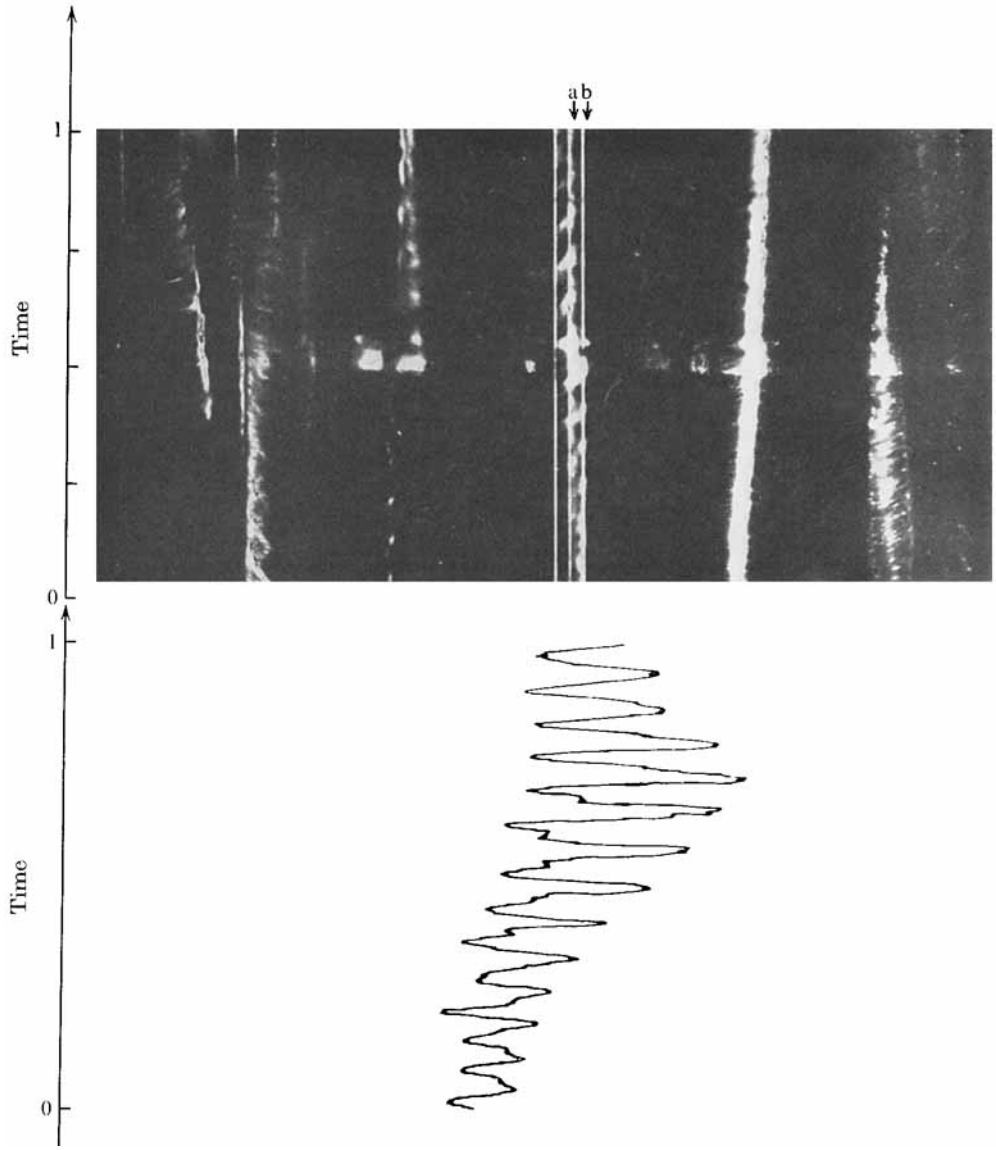

FIGURE 7. (x, t) photograph synchronized with thermocouple signal. The photograph shows bright regions flowing past the thermocouples labelled a and b. The trace shows the temperature difference between the thermocouples a and b for the same time period.